

RESOLVING THE UNRESOLVED COSMIC X-RAY BACKGROUND IN THE *CHANDRA* DEEP FIELDS

RYAN C. HICKOX¹ AND MAXIM MARKEVITCH¹

Accepted for publication in Astrophysical Journal Letters

ABSTRACT

We present a measurement of the surface brightness of the cosmic X-ray background (CXB) in the *Chandra* Deep Fields, after excluding all detected X-ray, optical and infrared sources. The work is motivated by a recent X-ray stacking analysis by Worsley and collaborators, which showed that galaxies detected by *HST* but not by *Chandra* may account for most of the unresolved CXB at $E > 1$ keV. We find that after excluding *HST* and *Spitzer* IRAC sources, some CXB still remains, but it is marginally significant: $(3.4 \pm 1.4) \times 10^{-13}$ ergs cm⁻² s⁻¹ deg⁻² in the 1–2 keV band and $(4 \pm 9) \times 10^{-13}$ ergs cm⁻² s⁻¹ deg⁻² in the 2–5 keV band, or $7\% \pm 3\%$ and $4\% \pm 9\%$ of the total CXB, respectively. Of the 1–2 keV signal resolved by the *HST* sources, $34\% \pm 2\%$ comes from objects with optical colors typical of “normal” galaxies (which make up 25% of the *HST* sources), while the remaining flux comes from objects with colors of starburst and irregular galaxies. In the 0.65–1 keV band (just above the bright Galactic O VII line) the remaining diffuse intensity is $(1.0 \pm 0.2) \times 10^{-12}$ ergs cm⁻² s⁻¹ deg⁻². This flux includes emission from the Galaxy as well as from the hypothetical warm-hot intergalactic medium (WHIM), and provides a conservative upper limit on the WHIM signal that comes interestingly close to theoretical predictions.

Subject headings: methods: data analysis — X-rays: diffuse background — X-rays: galaxies

1. INTRODUCTION

The cosmic X-ray background (CXB) is known to be primarily the integrated emission from X-ray point sources, mostly active galactic nuclei (e.g., Hasinger et al. 2005; Bauer et al. 2004). Recent studies have shown that the *Chandra* Deep Fields (CDFs) North and South, the most sensitive observations of the X-ray sky to date, resolve $\sim 80\%$ of the extragalactic CXB at 1–2 keV (Moretti et al. 2003; Worsley et al. 2005; Hickox & Markevitch 2006, hereafter HM06), and $\sim 50\%$ at 7 keV (Worsley et al. 2005). While the majority of the CXB at $E < 5$ keV has been accounted for, the nature of the still-unresolved component (the absolute intensity of which we derived in HM06) remains unclear.

Part of the unresolved CXB is due to faint point sources that have yet to be detected in X-rays. However, HM06 showed that an extrapolation of the observed $\log N / \log S$ curve to zero fluxes falls far short of the unresolved CXB. To account for it, the slope of the relation must steepen below the CDF-N X-ray source detection limit of $S_{0.5-2 \text{ keV}} = 2.4 \times 10^{-17}$ ergs cm⁻² s⁻¹. This is not implausible; Bauer et al. (2004) showed that the CDFs contain a population of normal and starburst galaxies with $S_{0.5-2 \text{ keV}} < 10^{-16}$ ergs cm⁻² s⁻¹ whose $\log N / \log S$ is indeed steeper, and which should dominate the source counts at $S_{0.5-2 \text{ keV}} < 10^{-17}$ ergs cm⁻² s⁻¹. These faint sources, while not detected in X-rays, can be associated with optical or infrared sources found in the CDFs. A recent X-ray stacking analysis of *Hubble Space Telescope* (*HST*) sources in the CDFs has found that their X-ray emission can account for most of the unresolved $E = 1 - 6$ keV CXB (Worsley et al. 2006).

Still, some of the unresolved flux should be truly diffuse. At $E < 1$ keV, there is flux from the Local Bubble (Snowden 2004) as well as charge exchange local to the Sun (e.g., Cravens 2000; Wargelin et al. 2004). In addition, some signal may come from the warm-hot intergalac-

tic medium (WHIM) with temperatures $10^5 - 10^7$ K, that is thought to comprise the majority of the baryons in the local Universe (e.g., Cen & Ostriker 1999; Davé et al. 2001). Models of the WHIM predict a signal dominated by line emission from oxygen and iron with prominent lines at 0.5–0.8 keV, but some flux up to 1.5 keV (Phillips et al. 2001; Fang et al. 2005; Ursino & Galeazzi 2006). To date the WHIM has proved challenging to observe, although there have been reports of detections of WHIM X-ray absorption lines (e.g., Nicastro et al. 2005, however see Kaastra et al. 2006), as well as excess soft X-ray emission around galaxies that has been attributed to the WHIM (e.g., Softan 2006). Diffuse emission could also come from more exotic sources such as decay of dark matter particles (e.g., Abazajian et al. 2007).

In this Letter, we constrain the diffuse CXB by directly measuring its absolute intensity in deep *Chandra* pointings after the removal of all sources detected in deep X-ray, optical, and IR observations. Our analysis is complementary to that of Worsley et al. (2006), and is a follow-up to HM06, in which we excluded only the X-ray sources.

2. DATA

Chandra X-ray observations of the CDFs North and South (CDF-N and CDF-S) have respective total exposure times of roughly 2 Ms and 1 Ms. The CDF-N data consist of two subsets, observed in Very Faint (VF) or Faint (F) telemetry mode. Each of the three subsets (CDF-N VF, CDF-N F, and CDF-S) contains 6 to 9 individual observations with exposure times 30 to 170 ks each. The datasets are identical to those used in HM06, except for the ACIS calibration updates. For subtraction of the instrumental background, we add the latest ACIS stowed observations, for a total background exposure of 325 ks, compared to 256 ks used in HM06. These updates caused no significant change to the CXB fluxes.

In HM06, we measured the CXB intensity after excluding X-ray detected sources from the catalog of Alexander et al. (2003). To further exclude the contributions of X-ray faint objects, we use sources detected in the optical and IR ob-

¹ Harvard-Smithsonian Center for Astrophysics, 60 Garden Street, Cambridge, MA 02138; rhickox@cfa.harvard.edu, maxim@head.cfa.harvard.edu.

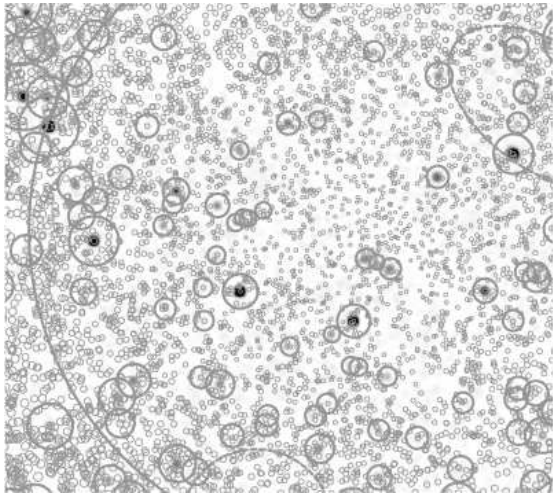


FIG. 1.— Smoothed 0.5–8 keV image of CDF-N, showing the source exclusion regions. The large circle is the 3.2' extraction region, medium-size circles and ellipses show X-ray point and extended sources, and small circles show *HST* sources.

servations of the Great Observatories Origins Deep Survey (GOODS, Dickinson et al. 2003). Optical and near-IR data were taken using the Advanced Camera for Surveys (ACS) on *HST* in the B_{435} , V_{606} , i_{775} , and z_{850} bands (Giavalisco et al. 2004). We use the public catalog² based on detections in the z_{850} band ($\lambda \sim 8300\text{--}9500\text{ \AA}$), with a limiting magnitude of $z_{850} \simeq 27$. The *HST* catalogs for CDF-N and CDF-S each contain ~ 4500 objects within the area for which we extract CXB spectra (inside a 3.2' circle, and away from detected X-ray sources, see § 3).

We also exclude sources detected with the Infrared Array Camera (IRAC) on *Spitzer*, in four bands centered on 3.6, 4.5, 5.8, and 8 μm . There is no published catalog currently available for these sources, so we have performed our own source detection using the calibrated IRAC images³. Sources were detected using the `SEXTRACTOR` code (Bertin & Arnouts 1996) in all four bands. In the most sensitive band (3.6 μm), we detect ~ 1000 sources in the X-ray extraction region to a 5σ limiting flux of $\sim 0.2\ \mu\text{Jy}$. Most ($>95\%$) of the IRAC sources have counterparts within $1''$ in the *HST* z_{850} catalog.

We also considered *Spitzer* Multiband Imaging Photometer (MIPS) 24 μm sources² and for CDF-N, Very Large Array (VLA) 21 cm sources (Richards 2000), with limiting fluxes of 80 and 40 μJy , respectively. All the sources within our X-ray extraction regions have *HST* or IRAC counterparts, except for 2–4 of the 80–90 MIPS sources and 1 of the 6 VLA sources, so we do not include these data in the analysis.

3. ANALYSIS

We calculate the CXB surface brightness as discussed in detail in § 5 of HM06, with only minor differences. For the *HST* and IRAC sources not detected in X-rays, we use smaller exclusion regions with radii equal to r_{90} , the X-ray point-spread function (PSF) 90% enclosed flux radius at 1.5 keV (see Eqn. 1 of HM06), compared to $4.5\text{--}9r_{90}$ for X-ray detected sources. Due to the large number of optical and IR sources, at large off-axis angles there is little area remaining after source exclusion. Therefore we only extract spectra from a circle around the optical axis with radius 3.2' (where $r_{90} = 2.2''$), compared

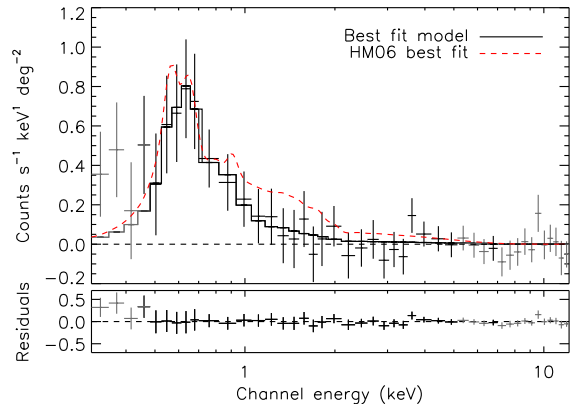


FIG. 2.— CXB spectrum for the CDF-N VF subset, with all sources (*Chandra*, *HST* and IRAC) excluded. The spectrum is fit with an APEC model with $kT = 0.20$ keV plus a power law with $\Gamma = 1.5$. Black points show the data included in the fit (see HM06), and the red dashed line shows the best-fit model for the CDF-N VF spectrum excluding only X-ray sources (HM06).

TABLE 1
CXB SURFACE BRIGHTNESS AFTER EXCLUDING ALL SOURCES

Energy (keV)	CDF-S	CXB intensity ^a CDF-N (VF+F)	Average	CXB frac. ^b (%)
0.5–2 ^c	45 ± 8	41 ± 11 ^d	43 ± 7 ^d	...
0.65–1 ^c	11 ± 2	9 ± 3 ^d	10 ± 2 ^d	...
1–2	5.0 ± 1.8	2.4 ± 1.6	3.4 ± 1.4	7.3 ± 3.0
1–1.3	1.7 ± 0.7	1.0 ± 0.7	1.3 ± 0.6	8.3 ± 3.8
2–5	7 ± 12	2 ± 10	4 ± 9	4 ± 9
2–8	14 ± 39	4 ± 30	7 ± 26	4 ± 16

^a Units are 10^{-13} ergs cm^{-2} s^{-1} deg^{-2} , errors are 68%.

^b Percent of total CXB, assuming a power-law CXB spectrum with $\Gamma = 1.4$ and normalization 10.9 ± 0.5 photons cm^{-2} s^{-1} sr^{-1} keV^{-1} at 1 keV (HM06).

^c Intensities for $E < 1$ keV are dominated by Galactic and local line emission that varies with time and position. These are not extragalactic values.

^d Does not include CDF-N VF, to exclude the local temporary excess.

to 5' in HM06. The solid angle we use here is 0.45 of that in HM06 when we exclude only X-ray sources, and 0.32 when we exclude all *HST* and IRAC sources.

For each of the datasets, we fit the spectrum of the remaining area with a model consisting of an optically-thin thermal component (APEC) with solar abundances and $kT \simeq 0.15\text{--}0.2$ keV, to account for emission from the Galaxy as well as any diffuse thermal CXB. We also include a power law component that dominates at $E > 1$ keV, and fix the photon index at $\Gamma = 1.5$, the best-fit value from HM06 (we do not vary Γ as in HM06, due to poorer statistics). These models do not necessarily provide a physical description of the emission, but they are sufficient for our purpose of calculating fluxes. A CDF-N VF spectrum with the model fit is shown in Fig. 2.

For each spectrum, we calculate fluxes in the 0.5–2 keV, 1–2 keV, 2–8 keV, and 2–5 keV bands, as well as the 0.65–1 keV and 1–1.3 keV bands, where the hypothetical WHIM signal or galaxy group emission are best distinguished from the diffuse Galactic foreground (see § 5.2). Errors on the observed flux include statistical errors in the sky and background count rates, and a 2% systematic uncertainty in the background normalization (§ 4 of HM06). We carefully ac-

² http://archive.stsci.edu/pub/hlsp/goods/catalog_r1/h_r1.1z_readme.html

³ http://data.spitzer.caltech.edu/popular/goods/Documents/goods_dataproducts.html

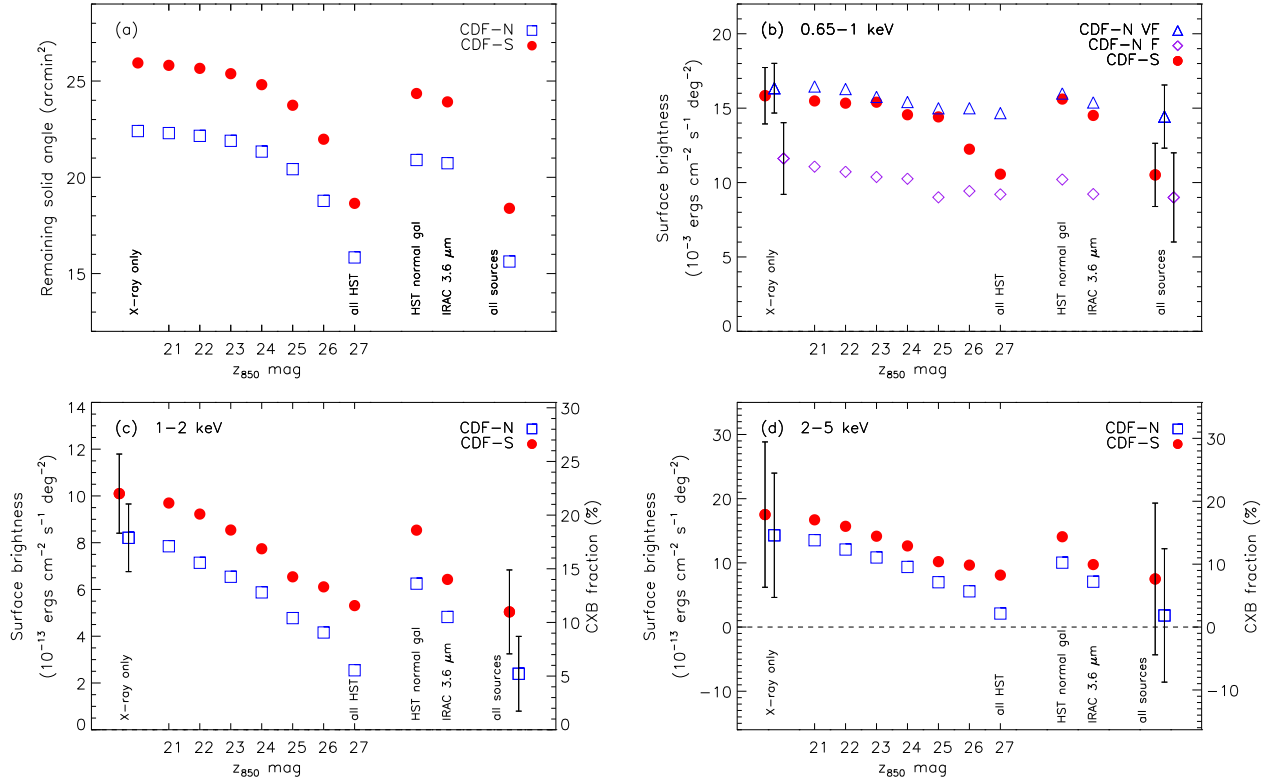


FIG. 3.— (a) Solid angles of the X-ray extraction regions, and (b–d) unresolved CXB surface brightness, for subsets of excluded *Chandra*, *HST*, and IRAC sources. In all panels, points on the far left show the value when only X-ray sources are excluded (as in HM06, but using the smaller $3.2'$ region). Points with z_{850} labels on the x-axis correspond to the additional exclusion of *HST* sources brighter than z_{850} (note that $z_{850} = 27$ is only an approximate detection limit for all *HST* sources). Points on the right show intensities excluding X-ray sources plus only *HST* “normal” galaxies (§ 5.1), only IRAC $3.6 \mu\text{m}$ sources, and finally all *HST* and IRAC sources. For the 0.65–1 keV band we show the CDF-N VF and CDF-N F subsets separately, as time variability in the local emission (apparently charge exchange in the Solar wind, e.g., Wargelin et al. 2004) caused these intensities to differ. For clarity, errors are shown only on the far left and right points. For (c) and (d), on the right axis we show the corresponding fraction of the total CXB, for which we assume a power law spectrum with $\Gamma = 1.4$ and normalization $10.9 \text{ photons cm}^{-2} \text{ s}^{-1} \text{ sr}^{-1}$ at 1 keV (HM06).

count for background uncertainties. Because of differences in pointing of up to $2'$ and the small X-ray extraction area, the composite stowed background spectrum includes 3 times (for CDF-N) and 1.5 times (for CDF-S) as many statistically independent photons as do the spectra for each separate observation. We accordingly increase the effective background exposure times by these factors. We conservatively neglected this effect in HM06, as it was much smaller due to the larger extraction area and fewer excluded sources.

A further small correction is necessary to subtract the point source flux that is scattered outside our exclusion regions. For each *HST* or IRAC source, 10% of the X-ray flux should lie outside r_{90} . However, because many regions overlap, the contribution of this scattered flux is smaller. Using a model of the *Chandra* PSF, we estimate that when all *HST* and IRAC sources are excluded with radius r_{90} , 5% (0.5–2 keV) and 8% (2–8 keV) of their flux should remain in our unresolved spectrum. Likewise, 0.3% and 0.6% of the flux from detected X-ray sources (for which we use larger exclusion regions) will be scattered into the spectrum. We account for both these small contributions in the final unresolved intensities. As a check, we tried exclusion regions of radius $1.5r_{90}$ and obtained identical results.

4. RESULTS

We first calculate the CXB intensity after excluding *HST* subsamples with various limiting magnitudes from $z_{850} < 21$ –

26, and finally excluding all *HST* sources ($z \lesssim 27$). We also try excluding only “normal” galaxies, selected based on their *HST* colors (see § 5.1), only IRAC $3.6 \mu\text{m}$ sources, and finally all *HST* and IRAC sources. In every case we also exclude all detected X-ray sources. The results are shown in Fig. 3, and the residual CXB intensities excluding all sources are given in Table 1. We also calculate the mean CXB intensity for all three subsets, including a detailed error analysis as described in § 8.2.3 of HM06.

Fig. 3 shows that excluding faint *HST* sources has little effect on the CXB at $E < 1$ keV, where it is dominated by the truly diffuse Galactic and local emission. At $E > 1$ keV, as fainter objects are excluded, the surface brightness of the CXB decreases, indicating that the *HST* sources do indeed contribute to the X-ray unresolved CXB. In the 1–2 keV band, the remaining intensity after excluding all *HST* and IRAC sources is above zero at only 1.5σ for CDF-N and 2.8σ for CDF-S. The CXB intensity decreases even as we excluded the faintest *HST* sources, suggesting that if we were able to go slightly deeper, we would resolve the 1–2 keV CXB to within our absolute uncertainties. The X-ray undetected *HST* sources contribute 1–2 keV intensities of $(5.7 \pm 0.3) \times 10^{-13}$ and $(4.3 \pm 0.3) \times 10^{-13} \text{ ergs cm}^{-2} \text{ s}^{-1} \text{ deg}^{-2}$ in CDF-N and CDF-S, respectively, or $59\% \pm 9\%$ and $45\% \pm 7\%$ of the unresolved CXB from HM06. The fluxes resolved by *HST* sources (given here and in § 5.1) represent *differences* between the points in Fig. 3, and do not depend strongly on

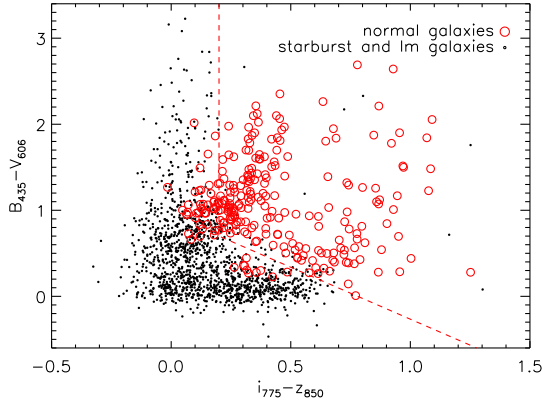


FIG. 4.— Color selection of “normal” galaxies from *HST* data. All points show $B_{435} - V_{606}$ vs. $i_{775} - z_{850}$ colors for sources in the UDF with $z_{850} < 27$. Sources are classified as elliptical and spiral galaxies (red circles) or starburst and Im galaxies (black dots) from photo- z analysis (Coe et al. 2006). Lines show our criteria to select “normal” galaxies from the GOODS data.

the instrumental background. Thus their errors are much smaller than the uncertainties on the absolute surface brightness shown in Fig. 3. Stacking the X-rays from the same *HST* sources, Worsley et al. (2006) found larger intensities of $(8.4 \pm 0.5) \times 10^{-13}$ and $(9.3 \pm 0.7) \times 10^{-13}$ ergs cm $^{-2}$ s $^{-1}$ deg $^{-2}$ for CDF-N and CDF-S, respectively. The cause of this difference is not immediately clear, but may be related to different accounting for overlap between the *HST* source regions.

In the 2–5 keV band, the *HST* and IRAC sources account for the entire unresolved CXB within the large absolute uncertainties. Similarly, Worsley et al. (2006) found that the stacked flux from *HST* sources is consistent with completely resolving the 2–6 keV CXB.

5. DISCUSSION

5.1. Which sources resolve the CXB?

Bauer et al. (2004) and HM06 show that AGN likely contribute a relatively small fraction of the CXB at X-ray fluxes below the CDF limit, where the X-ray source population is dominated by starburst and normal galaxies. To determine what class of galaxies gives the largest contribution to the unresolved CXB, we use *HST* colors to approximately divide the z_{850} sources into two subsets by galaxy type. While we do not have optical classifications for the *HST* GOODS galaxies, such a classification exists for the *HST* Ultra Deep Field (UDF), which covers a small region roughly 3' from the CDF-S aimpoint with a flux limit of $z_{850} \simeq 30$. The UDF was observed in the same four ACS bands as the wider GOODS fields, and Coe et al. (2006) performed a detailed photometric redshift analysis of the UDF sources, which classified each galaxy with one of eight templates (elliptical, Sab, Sbc, Im, and four types of starburst).

In Fig. 4, we show $B_{435} - V_{606}$ vs. $i_{775} - z_{850}$ colors for Coe et al. (2006) sources with $z_{850} < 27$, corresponding to the flux limits of the larger GOODS fields. In this diagram, normal (elliptical and spiral) galaxies occupy a different region from starburst and Im galaxies, with approximate boundaries $i_{775} - z_{850} = 0.2$ and $B_{435} - V_{606} = 0.9 - (i_{775} - z_{850})$, as shown in Fig. 4. Of the 255 “normal” galaxies in the UDF sample, 201 (73%) are in this region, while only 52 (21%) of the 253 galaxies in this region have starburst or Im classifications and would be mis-classified by this criterion. In the GOODS catalog, these criteria classify 25% of z_{850} sources as “normal”

galaxies and 70% as “starburst/Im” objects (5% of the sources do not have detections in all four ACS bands). The “normal” galaxies contribute $34\% \pm 2\%$ of the 1–2 keV intensity resolved by all the *HST* sources, and so have higher average X-ray fluxes than other X-ray undetected *HST* objects.

We also examine the contribution from the 3.6 μ m sources, which are on average only 0.25 magnitudes brighter in z_{850} than the *HST* sources, but account for a disproportionately large fraction of the unresolved CXB. The ~ 1000 3.6 μ m sources contribute $63\% \pm 2\%$ of the total 1–2 keV CXB resolved by all *HST* and IRAC sources. In comparison, the 1000 brightest *HST* sources (which have $z_{850} < 24.5$, and of which only 20% are IRAC sources) account for $53\% \pm 2\%$. Therefore, the X-ray flux from undetected X-ray sources is apparently more highly correlated with 3.6 μ m flux than with z_{850} flux. This may be an important clue to the nature of these faint X-ray sources, although a detailed discussion is beyond the scope of this Letter. In a forthcoming paper, we will determine how bright these undetected sources can be in the X-rays and whether *Chandra* could detect them in a reasonable longer exposure.

5.2. Comparison to WHIM predictions

While most of the remaining CXB signal should be due to Galactic or local diffuse emission and unresolved X-ray point sources, our results provide conservative upper limits on emission from the WHIM (Cen et al. 2000 and later works). The brightest WHIM emission feature should be a redshifted O VII 0.57 keV line, but it cannot be distinguished from the bright Galactic O VII line without much better (~ 1 eV) spectral resolution. However, the hotter WHIM phases with $kT \sim 0.2 - 0.5$ keV would also emit significant Fe XVII lines at $E \approx 0.72 - 0.83$ keV (rest-frame). Thus, the ratio of WHIM emission to Galactic foreground (which is well-approximated by a $kT \approx 0.15 - 0.2$ keV thermal spectrum, Fig. 1) may be higher at $E \gtrsim 0.6$ keV.

We can compare our 0.65–1 keV signal to predictions from cosmological simulations. Fang et al. (2005) find WHIM intensities of $\sim 3 \times 10^{-8}$, 3×10^{-10} , and 3×10^{-14} ergs cm $^{-2}$ s $^{-1}$ deg $^{-2}$ toward a galaxy group, filament, and void, respectively. Roncarelli et al. (2006) obtained a sky-averaged 0.65–1 keV signal of 5×10^{-13} ergs cm $^{-2}$ s $^{-1}$ deg $^{-2}$ after excluding galaxy groups and clusters. (For these two works, we have approximately converted fluxes from 0.1–1 keV and 0.5–2 keV to 0.65–1 keV). The CDFs were selected to lie away from bright groups, but if they do not lie in voids, then our observed signal, $(1.0 \pm 0.2) \times 10^{-12}$ ergs cm $^{-2}$ s $^{-1}$ deg $^{-2}$, comes interestingly close to the above predictions. Galactic superwinds may increase the WHIM metallicity (Cen & Ostriker 2006), so the line emission may be even higher. At higher energies, our 1–2 keV signal is 15 times higher than the predicted sky-averaged WHIM intensity of 0.19×10^{-13} ergs cm $^{-2}$ s $^{-1}$ deg $^{-2}$ (Phillips et al. 2001), so does not give an interesting limit. For a more quantitative comparison, it will be necessary to excise the regions around individual galaxies in the WHIM simulations similarly to our analysis. With such a simulation, one may be able to place interesting constraints on the distribution and metallicity of the WHIM in the CDFs.

We thank J.P. Ostriker and L.A. Phillips for fruitful discussions, and the referee, Franz Bauer, for helpful comments. RCH was supported by NASA GSRP and Harvard Merit

Fellowships, and MM by NASA contract NAS8-39073 and *Chandra* grant G04-5152X.

REFERENCES

- Abazajian, K. N., Markevitch, M., Koushiappas, S. M., & Hickox, R. C. 2007, *Phys. Rev. D*, in press, astro-ph/0611144
- Alexander, D. M., et al. 2003, *AJ*, 126, 539
- Bauer, F. E., Alexander, D. M., Brandt, W. N., Schneider, D. P., Treister, E., Hornschemeier, A. E., & Garmire, G. P. 2004, *AJ*, 128, 2048
- Bertin, E. & Arnouts, S. 1996, *A&AS*, 117, 393
- Cen, R. & Ostriker, J. P. 1999, *ApJ*, 514, 1
- . 2006, *ApJ*, 650, 560
- Coe, D., Benítez, N., Sánchez, S. F., Jee, M., Bouwens, R., & Ford, H. 2006, *AJ*, 132, 926
- Cravens, T. E. 2000, *ApJ*, 532, L153
- Davé, R., et al. 2001, *ApJ*, 552, 473
- Dickinson, M., Giavalisco, M., & The GOODS Team. 2003, in *The Mass of Galaxies at Low and High Redshift*, ed. R. Bender & A. Renzini (Berlin; New York: Springer), 324
- Fang, T., Croft, R. A. C., Sanders, W. T., Houck, J., Davé, R., Katz, N., Weinberg, D. H., & Hernquist, L. 2005, *ApJ*, 623, 612
- Giavalisco, M., et al. 2004, *ApJ*, 600, L93
- Hasinger, G., Miyaji, T., & Schmidt, M. 2005, *A&A*, 441, 417
- Hickox, R. C. & Markevitch, M. 2006, *ApJ*, 645, 95
- Kaastra, J. S., Werner, N., Herder, J. W. A. d., Paerels, F. B. S., de Plaa, J., Rasmussen, A. P., & de Vries, C. P. 2006, *ApJ*, 652, 189
- Moretti, A., Campana, S., Lazzati, D., & Tagliaferri, G. 2003, *ApJ*, 588, 696
- Nicastro, F., et al. 2005, *Nature*, 433, 495
- Phillips, L. A., Ostriker, J. P., & Cen, R. 2001, *ApJ*, 554, L9
- Richards, E. A. 2000, *ApJ*, 533, 611
- Roncarelli, M., Moscardini, L., Tozzi, P., Borgani, S., Cheng, L. M., Diaferio, A., Dolag, K., & Murante, G. 2006, *MNRAS*, 368, 74
- Snowden, S. L. 2004, in *Soft X-ray Emission from Clusters of Galaxies and Related Phenomena* (Dordrecht; Norwell, MA: Kluwer Academic Publishers), 103
- Sołtan, A. M. 2006, *A&A*, 460, 59
- Ursino, E. & Galeazzi, M. 2006, *ApJ*, 652, 1085
- Wargelin, B. J., Markevitch, M., Juda, M., Kharchenko, V., Edgar, R., & Dalgarno, A. 2004, *ApJ*, 607, 596
- Worsley, M. A., Fabian, A. C., Bauer, F. E., Alexander, D. M., Brandt, W. N., & Lehmer, B. D. 2006, *MNRAS*, 368, 1735
- Worsley, M. A., et al. 2005, *MNRAS*, 357, 1281